Journal of Computational and Applied Mechanics, Vol. 5., No. 1., (2004), pp. 181–192

NUMERICAL ANALYSIS OF THE STRESS DISTRIBUTION IN AN ELECTRON BEAM WELDED WORM WHEEL

Michal Vorel and Erhard Leidich
Deptartment of Engineering Design, Technical University Chemnitz
Reichenhainer Str. 70, 09126 Chemnitz, Germany
michal.vorel@mbv.tu-chemnitz.de

[Received: November 11, 2002]

Dedicated to Professor József FARKAS on the occasion of his seventy-fifth birthday

Abstract. In this paper the finite element method was used to determine various stress states in an electron beam welded worm wheel. These are the residual stresses due to the welding process, stress redistribution after teeth milling and another stress redistribution under operation load. It turned out that the maximum principal stress takes up the tangential direction and not the radial direction as was originally assumed. Based on this, the initiation of cracks in the weld can be explained. Teeth milling and applied operation loading proved to have a limited influence on the resulting stress state. Using the time development of residual stresses, an improved welding technology to eliminate the residual stresses was proposed.

Mathematical Subject Classification: 74S05
Keywords: finite element method, residual stresses, worm wheel

1. Introduction

Welded parts often exhibit very complex strain that generally results from residual stresses and stresses from external loading. This is also the case of an electron beam welded worm wheel, the weld of which is strained due to the residual stresses and due to the cyclic loading from the gearing. The wheel is made of a steel hub (S355J2) and a bronze rim (CC484K, Figure 1), which utilizes advantageous wear features of bronze while saving material costs. However, there are always large cracks completely embedded in the weld [1], no matter what the weld depths is. Along with this problem area, a certain minimum thickness of the bronze rim must be considered to prevent tearing off the steel body during operation [2]. Therefore, extensive numerical analyses were performed to explain the form and impact of the arising residual stresses. The objective is rather complex, as the welded joint consists of two very different materials. Furthermore, the unusual round geometry of the weld in a wheel results in even more complicated residual stress fields.

Welding with an electron beam is successfully used in many applications [3]. One of its important advantages is a high energy concentration in the electron beam, which generally leads to low residual stresses in thin weldments. The stress state in thick weldments is, however, more complex and may result in high residual stressing

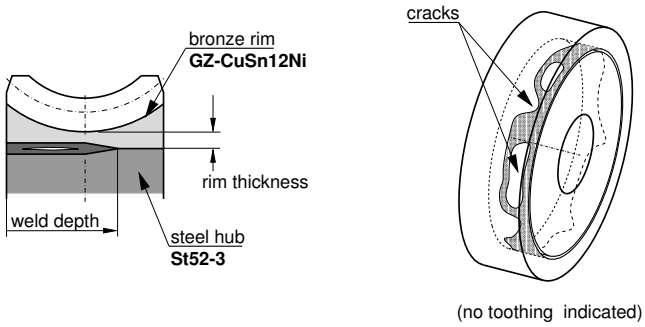

Figure 1. Cracks in an electron beam welded worm wheel.

induced thermally and by an unsuitable geometrical configuration. Residual stresses can be generally determined by numerical methods [4,5] or experimentally. In this paper the numerical method will be presented, as this enables a full description of the residual stressing in the wheel.

2. **Numerical Models**

For the analyses of stresses in the worm wheel the FE-method was used. The determination of residual stresses as a result of the welding process was achieved by an uncoupled thermal and structural analysis in the MARC program. In the thermal analysis the electron beam advance along the welding path was simulated to calculate the temperature fields. Those were used as boundary conditions in the subsequent structural analysis. The electron beam was modelled as a moving heat source of a rectangular volume. While there is a vacuum in the welding chamber, only cooling due to convection was modelled after the welding process was finished. The models used five different material zones [1].

Due to the temperature dependence of all material properties, the analyses were highly non-linear. The maximum temperature change in the thermal analysis was set for 20°C, which resulted in many analysis increments and consequently in large result files. Fine temperature steps were necessary for the following structural analysis, in which a maximum allowed temperature change lay at 50°C so that two or three increments of the thermal result file were used at once. It turned out that with other settings of temperature steps more iterations and hence longer computational time were needed to reach sufficient accuracy. The structural models used updated Lagrange formulation [6].

In order to further reduce computational costs geometric and mesh optimization of the models was carried out. Initially a complete worm wheel was analyzed (*C66*), as the resulting strain of the part is in general non-symmetrical. Because the analysis took even with a coarse mesh extreme computational time, another analysis with a pie wedge model (*W66-o*) was performed (Figure 2). It used simplified boundary conditions of a constrained displacement at the radial cuts. This induced an unreal

assumption that the radial boundary surfaces remain planar. However, in regions far

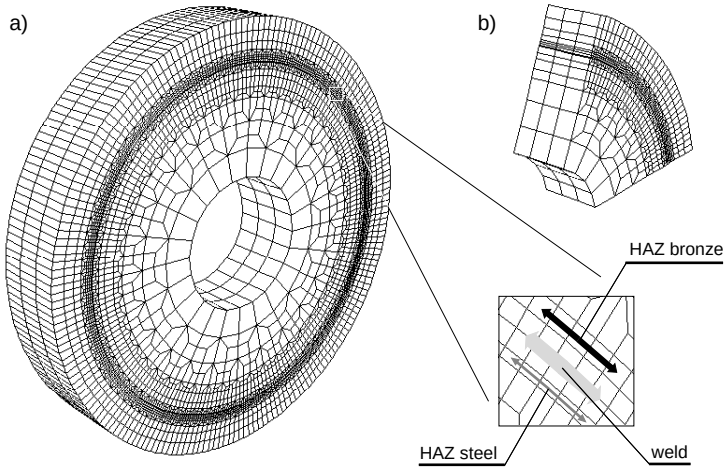

Figure 2. Coarse FE-meshes of a complete worm wheel with a detail of the weld (*C66*, a) and of a pie wedge model (*W66*, b)

enough from those surfaces results from the pie wedge model produced absolutely the same values as with the complete model (Figure 3). When using pie wedge models residual stresses agreed at a point far removed from the beginning of the weld as well as at a point of the weld overlap. With the geometrically reduced model a mesh optimisation was performed in order to make results independent of mesh density at a reasonable computational time. The degree of freedom (DOF) ranged from 8955 with the coarse model to 39207 with a fine meshed model. In the following analyses the medium fine mesh with 22485 DOF was used. One analysis parallel on two SGI R10000 computers took about 64 hours to finish.

3. **Residual Stresses after Welding**

In order to investigate residual stresses due to the welding process analyses with the pie wedge model in three variations of the weld depth were conducted using the following configurations:

- up to 66% of the wheel width welded model,
  - model out of the weld overlap (*W66-o*),
  - model at the weld overlap (*W66-a*),
- up to 80% of the wheel width welded model at the weld overlap (*W80-a*),
- up to 100% of the wheel width welded model at the weld overlap (*W100-a*).

The configuration with the weld overlap was mainly observed, as this region is critical for operation reliability.

As a result a full residual stress field at the weld overlap can be presented. In

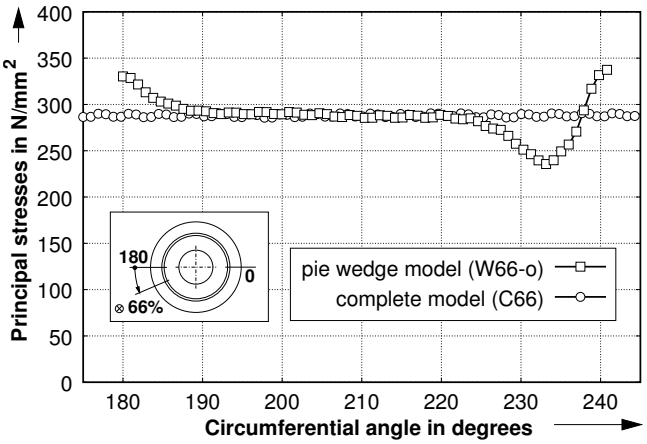

Figure 3. Maximum principal stress in the middle of the weld metal. Comparison of a complete model (*C66*) and a pie wedge model (*W66*).

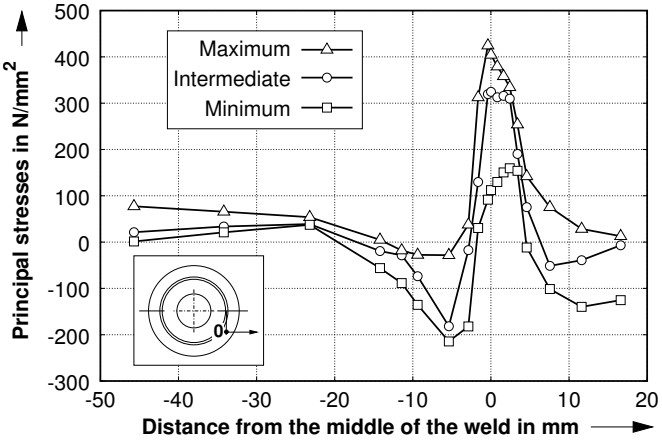

Figure 4. Principal residual stresses in the weld overlap along a radial path passing through the middle of the weld depth. Model *W66-a*

the middle of the weld (in radial direction) the maximum principal stress coincides mainly with the tangential direction. Similarly, the intermediate principal stress takes a predominantly axial direction and the minimum principal stress a radial direction. All principal stresses in the weld are positive. Shear stresses are almost zero in the whole wheel. In conclusion, the weld acts as a pre-stressed hoop. The equilibrium can only be established through negative stresses in the adjacent regions of the steel hub and the bronze rim, as can be seen in Figure 4. The course of principal stresses along the weld overlap shows an enormous fluctuation (Figure 5). This can be explained on the grounds of the time development of the maximum principal stress (Figure 6).

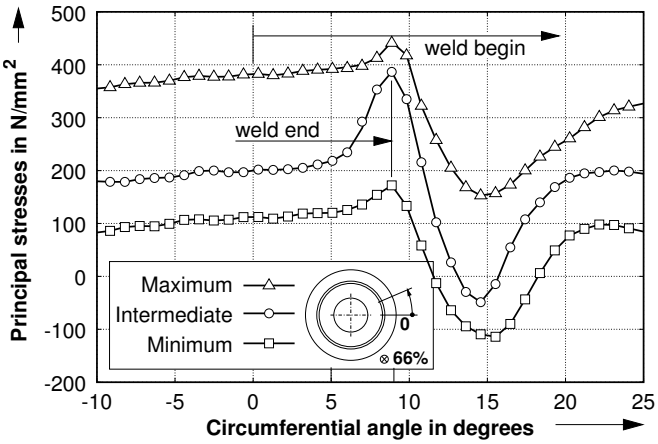

Figure 5. Principal residual stresses in the weld overlap along a tangential path lying in the middle of the weld depth. Model *W66-a*

After the first pass of the weld beam the stress rises with a high gradient. After the weld beam has passed along the whole wheel's circumference, the compressive stresses approach the tensile stresses of the already solidified weld seam and the ultimate stress difference reaches its maximum. With further advance of the weld beam reduction of the original tensile stresses takes place. This is caused by the frontal heat which leads initially to local annealing and subsequently to a full melting of the weld seam. After switching off, the weld beam goes forth for some more time, although it develops only little heat output. Therefore, the temperature field at the weld end does not spread uniformly during the final solidification process. Whereas during the welding process the generated heat is conducted mainly in radial directions from the weld seam, at the weld end the heat flux takes place in all directions. The end point cools down more quickly than the other regions and develops a local maximum of residual stresses. The stresses in front of the weld end are 'annealed' and do not recover any more to the high values. From a comparison of residual stress distribution for the considered models it can be concluded that the maximum stress levels virtually do not depend on the weld depth (Figure 7). The same conclusion can be drawn for the other primary stresses. Furthermore, residual stresses do not open the notch that exists in wheels with reduced weld depths. The deformed meshes show small mutual penetration of the elements at the crack faces, which implies crack closure due to compression forces. Therefore, unlike the original assumption about the mechanism of crack growth due to radial strain, the crack initiation and growth must depend on tangential strain. The crack initiation takes place probably at the weld end and approximately in the middle of the wheel width, where the principal stresses reach their highest values. This region is damaged by a large crack, which extends over the whole weld depth and crosses the weld root with up to 66% and 80% welded wheels. Along with this, the crack grows only in the middle of the weld thickness and propagates in the cylindrical plane

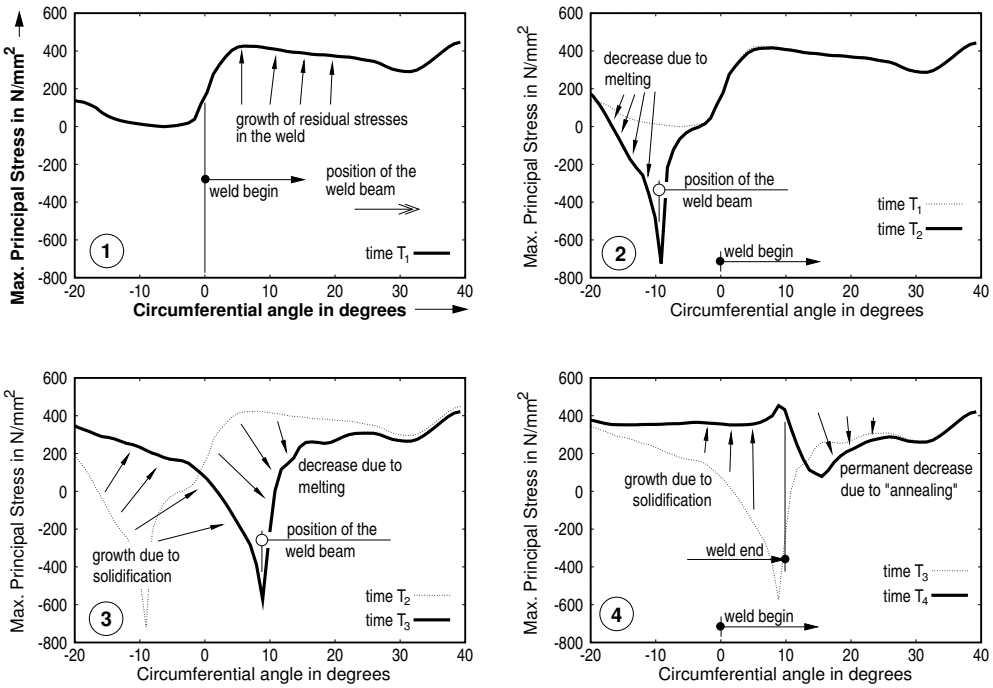

Figure 6. Time development of the maximum principal residual stress along a tangential path lying in the middle of the weld depth. Model *W66-a*

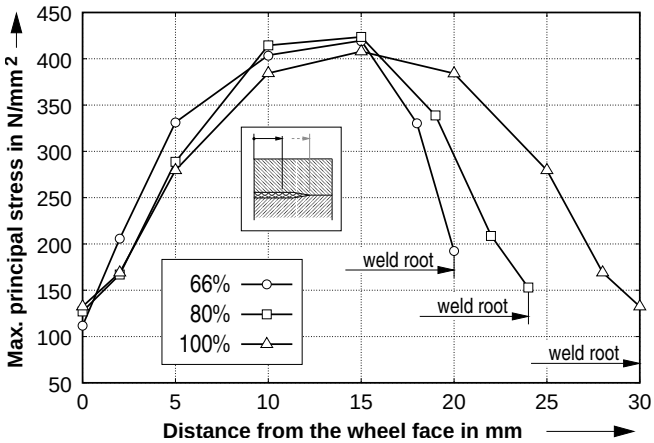

Figure 7. Maximum principal stress along an axial path lying in the middle of the weld depth. Models *W66-a, W80-a* and *W100-a*

coinciding with the weld. Whereas the stresses at the weld overlap are high in general and cause the crack to propagate through the whole wheel width, the stresses at other points of the weld cause only crack propagation in the middle of the wheel width and without any breaking through the weld root into the unwelded region. The stress peak along the weld depth stays in the middle of the wheel width, because the bronze rim thickness reaches its minimum there. Some preliminary numerical analyses have shown that with initiation of a small crack the maximum primary stress (as a hoop stress) has the effect of shear stress, i.e. the cracks grow due to Mode II and Mode III mechanisms. Since both heat affected zones show higher hardness, the crack is forced to remain fully within the weld material.

4. **Teeth milling impact**

After teeth milling the residual stress field changes. A simulation of this technological process was performed with the following models:

- up to 66% welded model at a point out of the weld overlap (*W66-om*),
- up to 66% welded model at a point of the weld overlap,
  - weld end under a tooth (*W66-amt*),
  - weld end under a tooth gap (*W66-amg*),
- up to 100% welded model at a point of the weld overlap (*W100-am*)

To analyze the stress distribution due to material ablation, the FE-meshes were built up with latent teeth. The geometry of tooth flanks was modelled only approximately. The simulation of the milling process was achieved by a gradual deactivation of elements within the tooth gaps. To keep the required accuracy only four analysis increments were needed. The analyses were performed with models cooled to 20°C. Residual stress fields were retrieved using the MARC restart files. The same numerical parameters were used during the analysis as previously. The results showed reduction of residual stresses in general. With the *W66-om* model the maximum principal stress reduces by approx. 50 N/mm^2 (Figure 8). The course of the stress along the welding path is sine shaped, with higher values under the tooth gaps. The course of the redistributed minimum principal stress has a similar shape. However, the stress peaks lie under the teeth and exhibit no decrease against the stress level before milling. The *W66-amt* and *W66-amg* models at the weld overlap proved little stress reduction at the weld end. This was particularly significant with the maximum principal stress. The stresses tended to acquire a similar sine course as above. The *W100-am* model showed only slightly higher stress levels then the *W66-amt* model. The intermediate principal stress reduced with all models by approx. 30 N/mm^2 and, unlike the other principal stresses, it showed very little fluctuation.

5. **Operation load impact**

After the simulation of teeth milling the external loading was applied to examine its influence on stress changes in the weld. Except for *W66-amg*, the same models as for the previous analysis were used. The related nominal loading of 825 Nm was

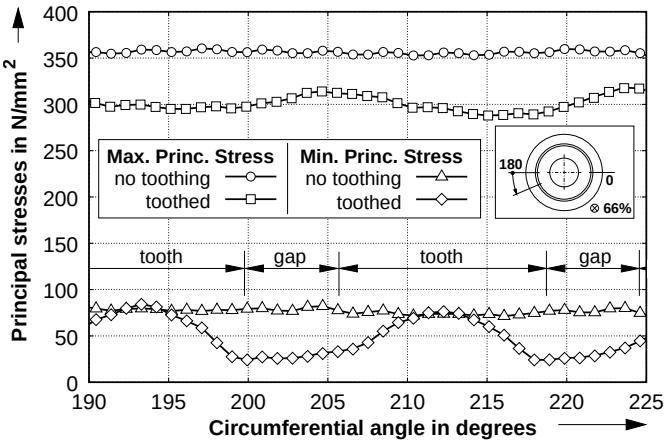

Figure 8. Teeth milling: redistribution of maximum and minimum principal stresses along a tangential path lying in the middle of the weld depth. Model *W66-om*

modelled by a distributed force on one tooth flank only. Although these conditions were rather exaggerated, there were only minor changes in the final stress in the weld. An example of the *W66-amt* model shows that the maximum and minimum principal stresses change by about 30 N/mm^2 at most (Figure 9). Because of tooth bending the

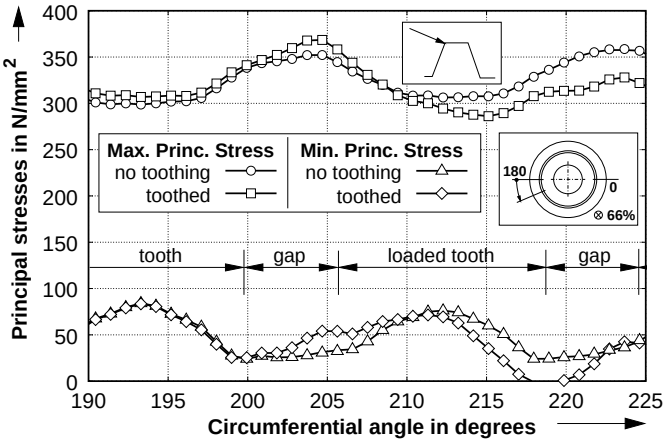

Figure 9. External loading: redistribution of maximum and minimum principal stresses along a tangential path lying in the middle of the weld depth. Model *W66-amt*

stresses decrease at the point under the loaded tooth flank and they get slightly higher at the point under the other flank of the loaded tooth. The elevated stresses do not

reach the values before the milling process in any way. The other models exhibited similar stress changes and there was almost no difference between the *W66-amt* and *W100-am* models. The intermediate principal stress did not change at all with any model. The results correspond well to the investigations made by Schmidt [2], where a stress change of maximum 25 N/mm^2 was determined using fine meshed models without residual stresses.

The important conclusion is that the stress levels in the weld reduce considerably and that they change little under the external loading. This means that the cracks in the weld, which are arrested right after the welding, become definitely stable after the milling process and also remain stable under the external loading. However, some ultrasonic tests have showen that the crack fronts are nonetheless strained up to the measure, which exceeds the threshold value necessary for a fatigue crack growth: the wheels after the operation exhibited larger cracks than before.

6. **Improved welding technology**

In general, welded components are often pre-heated before welding to prevent unwanted shrinking and high residual stresses which can also be eliminated by a subsequent stress-relief annealing. Worm wheels consisting of bronze can be pre-heated only up to limited temperatures. Refering to the ternary phase diagram Cu-Sn-Ni, the first phase change for the composition CuSn12Ni lies at 351°C [7]. Pre-heating beyond this temperature results in intensive hardening of the material, which is an unwanted feature for the weld as well as for the fatigue toughness of the teeth. Also some advantageous wear features would be irretrievably lost. Special stress-relief annealing could be introduced after the welding, but this would in no way dispose of the already existing cracks. Based on the numerical simulations, pre-heating of only 200°C is suggested so that the phase change temperature would not be exceeded in the whole rim during the welding process. Time development of the maximum principal stress in the weld of a pie wedge model out of the weld overlap shows that even a relatively small amount of pre-heating leads to some decrease of stress immediately after solidification (Figure 10). Due to natural cooling in the atmosphere after removal from the welding chamber, the maximum principal stress grows by about 70 N/mm^2. In this model the stresses in the weld capillary were not set to zero [8]. In results of test calculations the highly negative stresses return to the real values after about 1.2 seconds behind the weld beam. As can be seen, the residual stresses develop immediately after the weld solidification. This is caused by a highly concentrated electron beam heat source, which means steep temperature gradients and fast cooling of the weld by the bordering material regions (Figure 11). Thus, the intention is to slow down the cooling in the weld behind the welding beam. However, in an electron beam welding chamber this is a complicated objective, which can only be achieved by approximating the desired temperature course through applying several electron beams with gradually reducing power successively. In an optimum case this would result in keeping the residual stresses always at zero values. A splitting of an electron beam into several beams is possible without high additional costs. The trade-off for higher energy costs would be a safe worm wheel without any cracks at all.

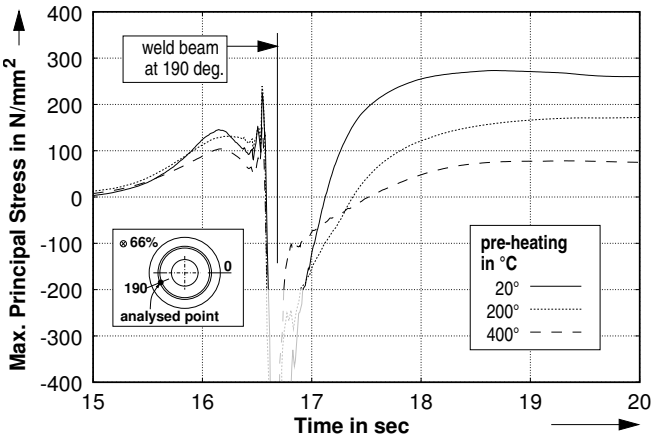

Figure 10. Time development of the maximum principal stress in the *W66-o* model under various pre-heating levels

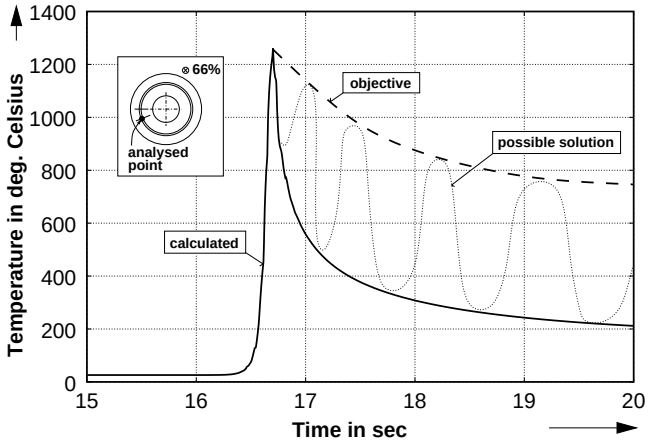

Figure 11. Time development of temperature in the *W66-o* model and desired improvements

To prove the benefits of the suggested welding technology, comprehensive numerical simulations were done with the *W66-o* pie wedge model while varying

- the number of electron beams (two, three or four),
- their intensity (100 to 30%), and
- the distance between them (3 to 15 mm).

To take advantage of pre-heating all models were considered at ambient temperature of 200°C. According to the above concept, the criterion for the optimized combination of the intensity and distance between the beams was that before the pass of the last

beam the maximum primary stress should never exceed its zero value. In order to find the optimum values for each number of beams, 16 simulations were done in a similar manner as above. It proved clearly that several concentrated electron beams following straight after each other with a 5 mm distance have a positive influence on residual stresses in the weld and in the neighboring regions. Directly after the solidification the maximum principal stress can be reduced by 220 N/mm^2 to 50 N/mm^2 when using four beams (Figure 12). This means that with a suitable subsequent cooling procedure the stresses would remain low and would not cause initiation of large cracks. To reach values of residual stresses near zero, many electron beams and therefore longer welding times would be necessary. However, this would be an inapplicable solution in terms of production costs. By welding with three or four beams the energy costs may rise considerably. However, with a perfect weld the wheel can be welded only up to 66%

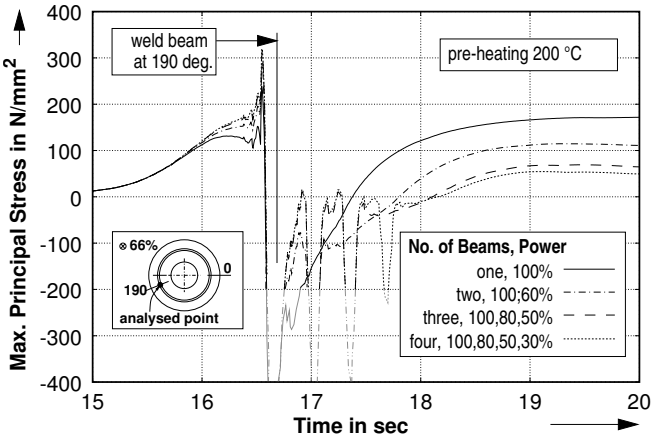

Figure 12. Time development of maximum principal stress in the *W66-o* model. Welding with one, two, three or four electron beams succesively

while taking advantage of safe operation and reduced bronze rim thickness.

7. **Conclusion**

In this paper theoretical work was done in order to explain stress distribution in an electron beam welded worm wheel in different states. Extensive numerical 3D analyses produced full residual stress field in an uncracked worm wheel. The calculated stress fields give a good explanation for the loci of most probable crack initiation. The important result is that crack growth depends predominantly on tangential stresses and not on the radial stresses as was originally assumed. Through the analysis of time development of residual stresses during the welding process an improved welding procedure was proposed to reduce residual stresses considerably or to prevent them completely. This is achieved by additional warming up the weld with more electron

beams following directly after the welding beam. This technology implies higher energy costs but as a compensation offers a perfectly welded worm wheel. Currently, experimental tests are being conducted to verify the numerical results and prove the new welding technology.

In further research some numerical analyses are planned to evaluate stability of cracks in the weld under external loading. For this purpose experimental work is also necessary to determine the threshold value for fatigue crack growth.

REFERENCES

1. Vorel, M. and Leidich, E.: *Impact of residual stresses on crack distribution in an electron beam welded worm wheel.* In Maschinenbau und Nanotechnik, 47. Internationales Wissenschaftliches Kolloquium, Ilmenau, 2002.
2. Schmidt, G.: *Untersuchungen zur Tragfähigkeit elektronenstrahlgeschweisster Schneckenräder.* Berichte aus dem Maschinenbau. Shaker Verlag, 1999, Aachen.
3. Schultz, H.: *Elektronenstrahlschweißen.* Fachbuchreihe Schweißtechnik. DVS Verlag, 2000, Düsseldorf.
4. Radaj, D.: *Schweissprozesssimulation: Grundlagen und Anwendungen.* Fachbuchreihe Schweisstechnik. Verlag für Schweissen und Verwandte Verfahren; 1999, DVS Verlag, Düsseldorf.
5. Voss, O.: *Untersuchung relevanter Einflußgrößen auf die numerische Schweißsimulation.* Forschungsberichte des Instituts für Schweißtechnik. Shaker Verlag, 2001, Aachen.
6. Zienkiewicz, O.C. and Taylor, R.L.: *The finite element method: Solid mechanics*, Volume 2. Butterworth-Heinemann, 2000, Oxford.
7. Guertler, W.: *Konstitution der ternären metallischen Systeme.* Kompendium, Heft 12., 1961, TU Berlin.
8. Lenz, B. and Rick, F.: *Lösungsansätze zur Simulation des Laserstrahlschweißens.* In Applications of Lasers and Electroptics, 1999, San Diego.